Development of the Electrical and Magnetic Model of Variable Reluctance Speed Sensors

Robert A. Croce Jr., Ph.D.[1], Igor Giterman[1]

[1]**Harco Laboratories**, 186 Cedar Street, Branford, CT 06405, USA

Abstract

This paper presents the electrical and magnetic analytical model as well as experimental validation of the output characteristics of variable reluctance speed sensors. The objective of this study is to develop a universal model which is capable of predicting the dynamic performance of speed sensors. This model will be used to further optimize existing speed sensor designs as well as aid in the development of new products. Experimental tests were performed and compared with the simulated results in order to validate the feasibility of the model. The simulated results of this sensor was shown to align within reason to the fabricated experimental characteristics, indicating that this model can be a powerful tool which has the potential to be applied across a vast majority of sensor designs. Furthermore, an equivalent electrical model has been developed which enables the suppression of higher order harmonic frequencies at the output, and to allow the sensor to operate at all desired frequencies without exceeding or falling below the voltage levels typically dictated by design requirements.

1. Introduction

Variable reluctance sensors are used to measure position and speed of moving ferrous objects. Their versatility, simplistic design and relatively low cost of manufacturability make them attractive for use in aerospace [1] and automotive [2] industries where it is desired to quantify the rotational speed of engine components such as crankshafts and turbines. The variable reluctance sensor consists of a permanent magnet and a ferromagnetic pole piece surrounded by a coil of wire. The sensor generates an analog voltage output signal when a ferromagnetic material passes by the tip of the pole piece. This induced voltage follows Faraday's Law of Induction, stated by the following equation as:

$$V = -N\frac{d\phi}{dt} \quad \textbf{(1)}$$

where N is the number of turns in the coil, ϕ the magnetic flux induced in the coil and t is the time elapsed during the change in magnetic flux. The magnitude of the induced voltage is therefore a direct function of the flux linkage in the coil as a function of time.

A powerful analytical design tool would enable the prediction of output voltages and transient waveform shapes as a function of physical parameters including, but not limited to, sensor component materials and sizes, gear tooth geometry, tooth spacing and gear material. The ability to accurately model dynamic sensor performance would enable the optimization of performance and cost of existing products, as well as aid in the design of new products and systems.

In this study, we have developed both a magnetic and electrical model of variable reluctance sensors which has shown good correlation to data collected from experimental sensors. The magnetic model can be primarily employed to model the transient electromagnetic response of the sensor, whereas the electrical model can be used to adjust the output to ensure noiseless and seamless interfacing with zero-cross detection and associated signal conditioning circuitry. For the purposes of this model, the ferromagnetic material consists of a toothed gear fabricated out of 430F solenoid quality stainless steel. For the magnetic simulation of this sensor a finite element analytical model was developed which allowed us to simulate the magnetic fields present around the sensor while rotating the test gear at discrete angular rotational steps. The flux linkage in the coil was then calculated at each rotation. Here, a MATLAB program was used to provide an automated testing environment which enabled full control over the finite element software as well as provided a means for data collection and analysis. Additionally, by knowing the discrete rotational time steps a transient waveform was reconstructed and compared with experimentally gathered waveform data.

2. Experimental Procedures

a. Fabrication of Test Gears

Two tests gears were created to analyze the effect of different tooth geometry on the signal output. 430F solenoid quality ferritic chromium-iron stainless alloy (Dunkirk Specialty Steel) was chosen as the gear material due to its high magnetic permeability, low residual induction and excellent corrosion resistance. The first gear fabricated had a total of 20

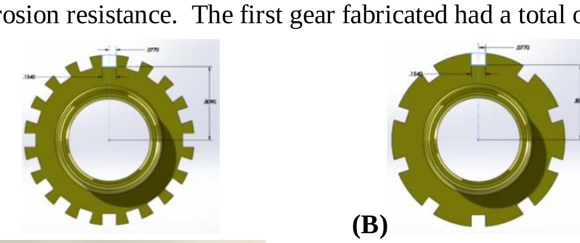

(A) **(B)**

(C)

Figure 1: **(A)** 430F testing gear with 20 teeth; **(B)** 430F testing gear with 10 teeth; **(C)** Photograph of fabricated gears.

Table 1: Measured Sensor Parameters.

Frequency (Hz)	Zs (Ω)	Phase (°)	Ls (mH)	Xs (Ω)	Rs (Ω)
100	90.49	9.28	22.80	14.35	89.36
120	91.05	11.06	22.90	17.23	89.40
1000	172.27	55.89	22.70	142.53	96.59
10000	1205.80	67.45	18.40	1112.60	462.70

teeth, equally spaced out 0.1540” over a diameter of 1.8739” with a depth of 0.25”. The second gear contained 10 teeth equally spaced out 0.1540” over the same 1.8739” with the same depth of 0.25”. The fabricated gears can be seen in Figure 1.

b. Fabrication of Speed Sensors

The sensor used for this study was a Harco fabricated high performance speed sensor. In short, the assembly consisted of a NdFeB permanent magnet (n4520), ferritic stainless steel pole piece (430FR) and a 1700 turn coil employing 39 AWG magnet wire surrounding the pole piece.

c. Material Characterization

1) *430F Annealing for Magnetic Properties* – Fabricated gears were annealed at 1500 °F for 2 hours then cooled 100 °F per hour to 800 °F. Surface oxidation of gears post-annealing was removed by sand blasting the finished part.
2) *Rockwell Hardness Evaluation* – B-scale Rockwell hardness values of 430F gears were evaluated before and after the annealing procedure by using a Wilson/Rockwell hardness tester. A hardness of 80 HRB and 78 HRB was measured before and after annealing, respectively.

d. Measurement of Sensor Parameters

Sensor inductance and resistance were measured using a QuadTech 1715 Digibridge LCR meter. Series resistance and inductance values were obtained at frequencies of 100, 120 1,000 and 10,000 Hz using 0.25V level measurement. Inductance and resistance measurements as a function of frequency can be seen in Table 1. It is noteworthy to mention that the true sensor inductance values become apparent at higher frequencies and true resistance values are taken under DC conditions. This yields L and R values of approximately 18 mH and 90 Ω, respectively.

e. Sensor Data Collection and Analysis

Experimental data was carried out using the SureServo Motor Driver with a SureServo Low/Medium Inertia Motor. The motor driver was programmed to achieve test gear speeds ranging from 600 RPM (200 Hz for the 20 tooth gear and 100 Hz for the 10 tooth gear) to 18,000 RPM (6,000 Hz for the 20 tooth gear and 3,000 Hz for 10 tooth gear). The output of the speed sensor was analyzed on a LeCroy Waverunner-2 Digital Oscilloscope, and raw transient data was recorded *via* RS-232 using the LeCroy ScopeExplorer Software for analysis and comparison to simulated data.

f. Simulation Software

Electromagnetic finite element simulations were performed and controlled using MATLAB. The electrical model was developed and simulated using OrCAD Capture.

3. Results and Discussion

a. Experimental Results

Figure 2 displays a cross-sectional representation of the sensor geometry and testing gear.

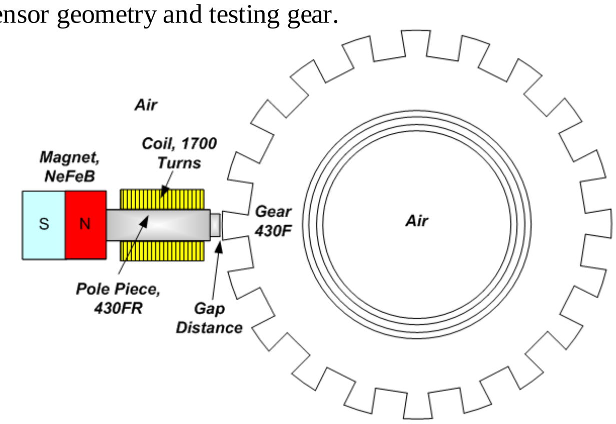

Figure 2: Cross-sectional representation of the speed sensor geometry and the 20 tooth testing gear.

As indicated in Section 1, the operational principle of this sensor is based on the changing magnetic flux as a function of time by passing a ferrous material by the pole piece tip. It can therefore be concluded that the magnitude of the magnetic field generated can be altered by the ferromagnetic properties of the testing gear. Henceforth, it would be imperative to quantify the effect the magnetic permeability has in determining the resultant magnetic field coupled into the coil.

It is known that magnetic characteristics of ferritic stainless steels can degrade after machining. Subsequent to gear fabrication, an annealing process was implemented to re-align the crystal lattice in order to achieve an even atomic structure and optimize the magnetic properties of the alloy. To quantify the effect this annealing has on the output characteristics, the sensor was tested before and after annealing, and the peak-to-peak voltages were compared. Figure 3 shows the peak-to-peak voltage as a function of frequency before (a), and after (b) annealing. As elucidated from the plots, the annealing protocol had a trivial effect on the induced magnetic field (i.e. peak-to-peak voltage), which resulted *ca.* 1-2% increase in magnitude. This increase of 1-2% can be considered negligible give that experimental errors due to gaping, component tolerance, coil winding and other assembly procedures have been observed to amount to approximately 5%.

a. Magnetic Model and Simulation

Finite element analysis used to model and simulate the output voltage generated by the sensor as a function of gear frequency. Figure 4 shows a static simulation of the sensor

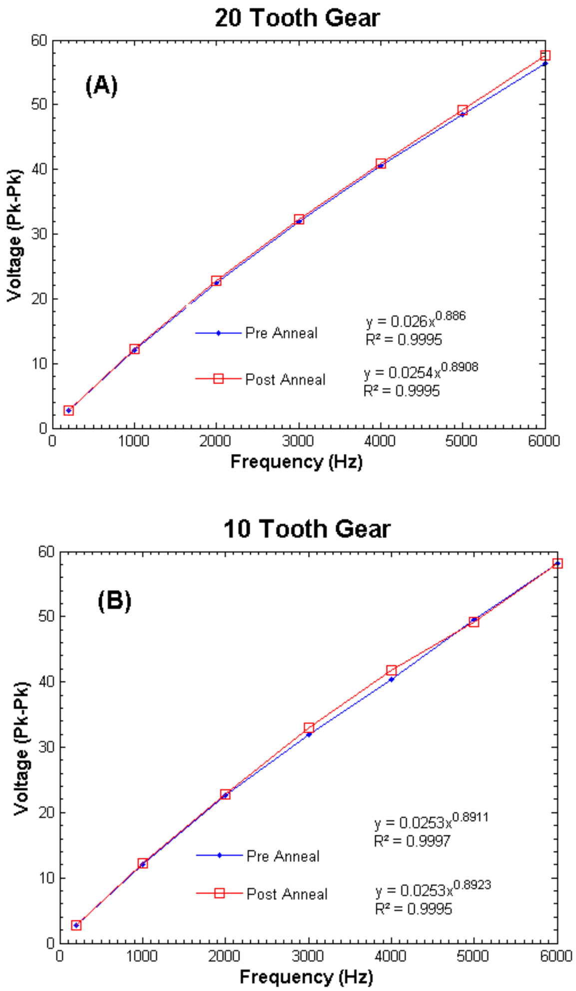

Figure 3: Effect of gear annealing (**(A)** 20 tooth gear, **(B)** 10 tooth gear) on sensor output voltage.

with the pole piece tip located in the center of the gear gap, with magnetic flux lines indicating the magnitude and direction of induced magnetic fields. The physical dimensions and electromagnetic parameters used in the simulation can be seen in Table 2.

MATLAB was used automate the simulation environment by rotating the test gear a discrete rotational steps, while capturing the flux linkage at each step. The flux linkage in the

Table 2: Simulation Parameters

	Material	Dimensions	Electromagnetic Properties
Magnet	NeFeB	0.4" x 0.328"	H_C = 1034507 A/m, μr = 1.05
Pole Piece	430FR	⌀ 0.150" x 0.500"	Non-linear BH Curve
Pole Piece Tip	430FR	⌀ 0.106" x 0.050"	Non-linear BH Curve
Coil	Cu Magnet Wire	39 AWG	n/a
Gear	430F	⌀ 1.8739"	Non-linear BH Curve

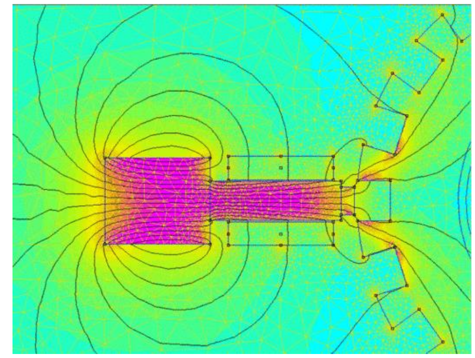

Figure 4: Simulation environment of the variable reluctance speed sensor.

coil was translated to peak-to-peak voltage by correlating the time step with Δϕ, per equation (1). The simulated output as a function of frequency when compared with experimental data can be seen in Figure 5. The red curve illustrates the experimental data and the blue curve the simulated data. It is noted that the experimental curve contains adverse physical electromagnetic phenomena such as Eddy currents and skin effects which can degrade performance. These effects have been observed and can be attributed to the slight deviation of experimental data from true linear operation (R^2 = 0.9995), which is observed in simulation (R^2 = 1). In an effort to compensate for this non-linear behavior at higher frequencies, the experimental curve was scaled by the varying inductance as a function of test frequency seen in Table 1, which is assumed to be caused by the presence of Eddy currents. By employing this scale factor, experimental data approaches linear operation (R^2 = 0.9999). The simulated data deviates an average of approximately 8% over the full range of frequencies tested (200 → 6,000 Hz).

Figure 6 illustrates the experimental *vs.* simulated transient response of the sensor with both testing gears. The simulated waveform reconstruction is able to closely simulate the experimental shape, indicating that accurate modeling of sensor transient shape has been achieved and is able to be used as an optimization tool for gear tooth sizing and spacing.

b. Electrical Model

The equivalent electrical circuit can be modeled as a series

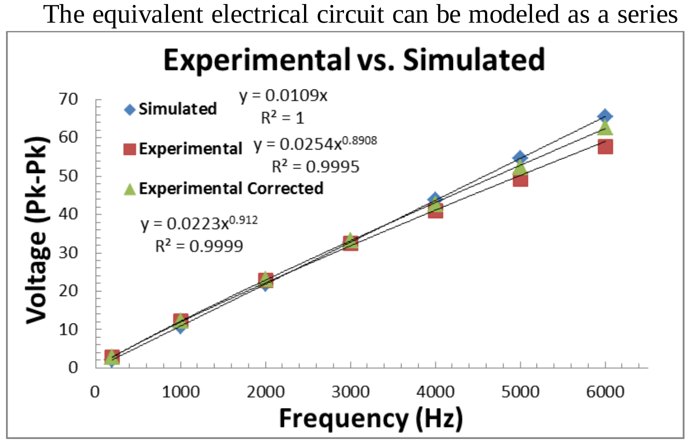

Figure 5: Experimental vs. simulated sensor curves.

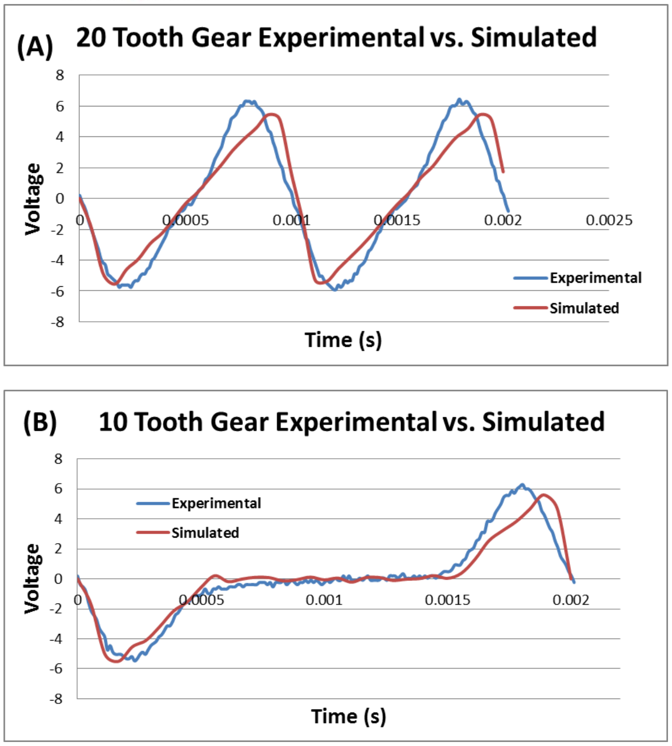

Figure 6: Experimental vs. Simulated transient waveform of the speed sensor.

RL circuit excited by a sinusoidal voltage source, as shown in Figure 7.

R_{Coil} and L_{Coil} are the internal resistance and inductance of the coil, respectively, and were obtained experimentally using a QuadTech 1715 Digibridge LCR Meter as discussed in Section 2 (d). The sinusoidal input voltage source, VAC, is modeled from open circuit experimental measurements (without Load Components). This is a valid design assumption given that under open circuit conditions, no closed loop current flows through either R_{Coil} or L_{Coil}. R_L and C_L represent the external load components which can be employed to adjust the output magnitude and/or resonant frequency of the signal over the full frequency range of the design.

Careful attention must be directed towards higher-order signal harmonics which are inherently present during periods of no magnetic flux generation, i.e. section of the gear containing a

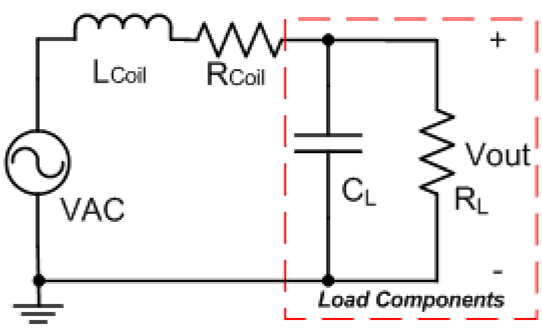

Figure 7: Equivalent circuit model of the variable reluctance sensor.

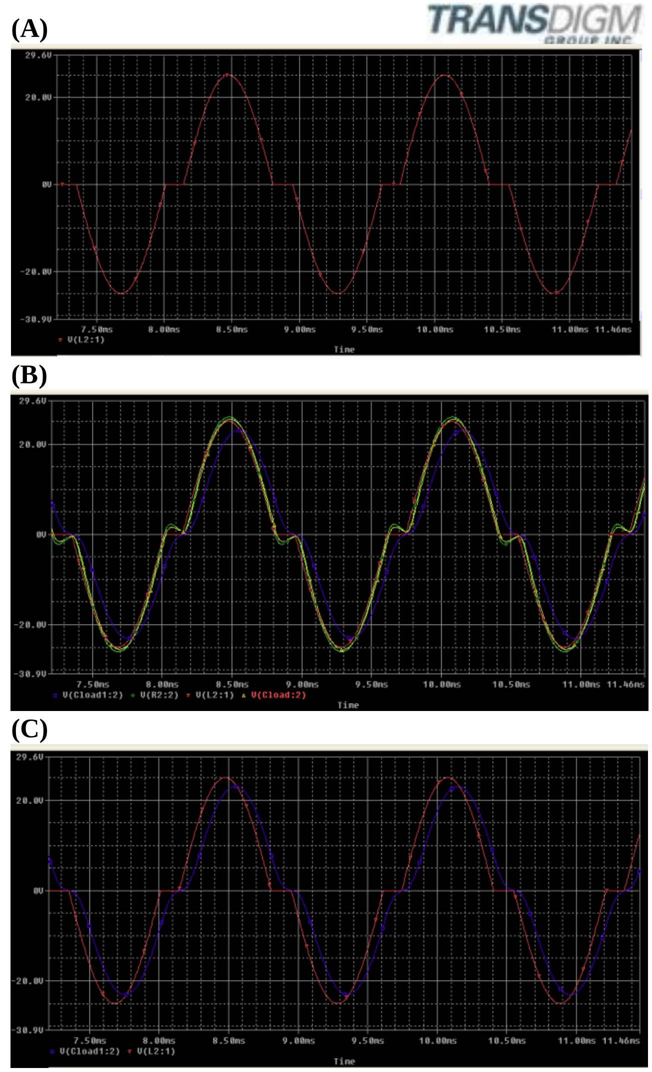

Figure 8: **(A)** Simulation of sensor sine wave; **(B)** Simulation of sensor input, unwanted frequency harmonics and the final output; **(C)** Sensor input and output alone.

large tooth and/or tooth spacing with respect to the width of the pole piece tip. These erroneous frequency harmonics about 0 V have been shown to be problematic due to the fact that the sensor's output signal will ultimately be connected to interfacing electronics and signal conditioning circuits which employ zero-cross detection. Harco's proprietary design eliminates the aforesaid higher order frequency components ensuring complete preservation of the sensor signal.

OrCAD was used to simulate the abovementioned frequency harmonics during these flat transient periods and the resulting signal after utilizing our design methodology. The sensor parameters used for the simulation were 18 mH and 90 Ω. Shown in Figure 8 (a) is the sine wave used as the source signal. Flat periods were introduced into the signal to simulate periods of no voltage generation to allow higher-order harmonics to be displayed. Figure 8 (b) shows the simulation result illustrating the frequency harmonics, traces yellow and green, present during periods of no voltage generation. The aforementioned oscillations were and the final output can be viewed as the purple trace. In Figure 8 (c), only the input and output signals were plotted.

As previously mentioned, the load components R_L and C_L of Figure 7 can be employed to adjust the resonant frequency point of the equivalent circuit. By utilizing the correct parallel R_L and C_L combination, the circuit's inherent resonant frequency behavior will limit the output voltage ensuring that the maximum voltage requirement will never exceed the peak-to-peak value at resonance. Additionally, it is noteworthy to mention that this design method ensures that voltage levels at low frequencies remains unaltered, thereby conforming to design specifications which typically specify a minimum and maximum amplitude and frequency range. Figure 9 illustrates experimental data showing this load capacitance effect on resonance. Here, it can be concluded that be choosing the right load capacitance value under the correct experimental conditions, a maximum voltage level is reached and is never exceeded under all experimental frequencies.

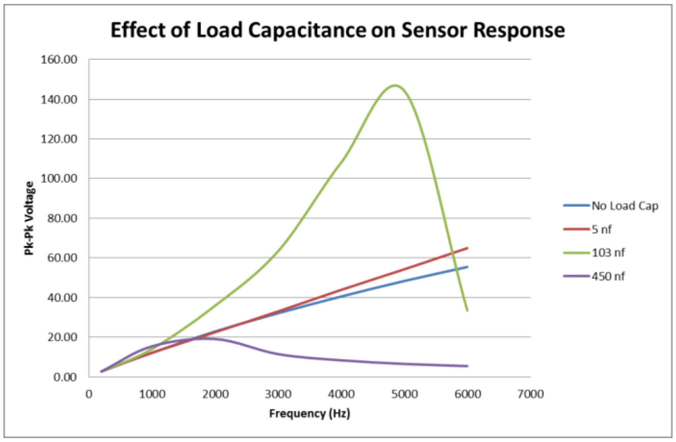

Figure 9: Experimental sensor output curves demonstrating the effect of load capacitance on resonance.

4. Conclusions

The results of the studies presented in this paper demonstrated an electrical and magnetic analytical model for variable reluctance speed sensors for aerospace applications. In terms of electromagnetic modeling, the simulation results fell within an average of 8% of experimentally collected data for frequencies up to 6,000 Hz. Overall, the simulated model correlated well with the experimental data given experimental variances such as sensor assembly (coil winding, magnet strength and dimensional tolerances), fabricated gear tolerances and testing procedures such as air gap setting.

In terms of the electrical model, we were able to simulate the effect of load resistance and capacitance has on sensor output. The ability to remove harmonic frequency generation from sensor signals gives us a huge leverage in design flexibility as we can now use equivalent circuit resonance to act as a self-limiting voltage clamp for all operating frequencies.

5. References

[1] Nebyloz, Alexander, *Aerospace Sensors*, Momentum Press, New York, NY, 2012.

[2] Erjavec, Jack and Thompson, Rob, *Automotive Technology: A Systems Approach*, Delmar Cengage Learning, 6th Edition, Clifton Park, NY, 2014.